ELSEVIER

Adhesion and friction behaviours of polydimethylsiloxane − A fresh perspective on JKR measurements

Vidya Vaenkatesan [a], Zhili Li [a], Willem-Pier Vellinga [b,1], Wim H. de Jeu [a,*,2]

[a] Dutch Polymer Institute and Department of Chemical Engineering and Chemistry, Eindhoven University of Technology, Eindhoven, The Netherlands
[b] Department of Mechanical Engineering, Eindhoven University of Technology, Eindhoven, The Netherlands

Abstract

The self-adhesion of a variety of polydimethylsiloxanes (PDMS) has been investigated using a newly developed JKR apparatus that can also determine the associated friction behaviour of the same sample. The results have been interpreted using the complete JKR model by incorporating the indentation data also in the analysis. By varying the molecular mass M_c of PDMS from 6 to 28 kg/mol the elastic modulus E decreases from 1.16 to 0.71 MPa while the work of adhesion remains about constant. In contrast measurements of the friction of the same systems indicate an increase of the friction force. Introduction of dangling chains leads to a strong decrease of E from 1.16 to 0.56 MPa for low M_c and from 0.71 to 0.09 MPa for high M_c and again only to minor changes in W. The latter results can be understood from an inward distribution of the dangling ends.
© 2006 Elsevier Ltd. All rights reserved.

Keywords: Siloxanes; Adhesion; Friction

1. Introduction

Adhesion is a phenomenon in nature with many complex sides. It plays a role in biofolding via cell adhesion and governs the surface properties of many materials. Regarding polymers, understanding the adhesion behaviour is imperative to their successful application in a variety of industrial applications. Since the pioneering work of Barquins *et al.* [1], the so-called JKR method [2,3] − based on the continuum contact model developed by Johnson, Kendall and Roberts − is widely popular for estimating the surface free energy and the work of adhesion between solids. One reason is that this technique minimizes the sample volume and thus reduces any bulk viscoelastic losses.

Some recent reviews are given in Refs. [4−6]. Adhesion corresponds to the thermodynamic work of adhesion of two bodies in contact. The adherence that refers to the mechanical energy required to separate them, differs from the adhesion energy because of, for example, bulk viscoelasticity, time dependent entanglement of polymer chains at the surfaces, or the formation of chemical bonds. Scientific interest and technological relevance arise from the ability to control surfaces by manipulating these energies, which requires methods to measure them accurately. The study of adhesion and adherence could also help understand friction, as the latter should be strongly influenced by the adhesive properties.

The literature is replete with reports on JKR investigations of the adhesion and adherence using elastomers, in particular polydimethylsiloxane (PDMS), as a model system. Studies of the influence of PDMS composition on the adhesion include changes in molecular crosslink density, surface-grafted chains, dangling chains and extraction [7−11]. Furthermore, effects of chemical modification of the PDMS surface on the adhesion behaviour have been reported. This includes deposition of self-assembled monolayers, hydrolyzation of the surface, and

---

* Corresponding author. Faculty of Chemical Engineering & Chemistry, Eindhoven University of Technology, P.O. Box 513, 5600 MB Eindhoven, The Netherlands. Tel.: +31 40 247 3772; fax: +31 40 243 6999.

E-mail address: w.h.dejeu@tue.nl (W.H. de Jeu).
[1] Present address: Department of Applied Physics, University of Groningen, Groningen, The Netherlands.
[2] Also at the FOM Institute for Atomic and Molecular Physics, Amsterdam, The Netherlands.

surface-treatment with UV/ozone [6,12–14]. Also the influence of the environment on adhesion behaviour has been investigated [15]. Most of these studies report an enhanced adherence with the modifications mentioned, as manifested by an increased hysteresis between loading and unloading curves. However, in other reports, under similar conditions no hysteresis was observed leading to a perfect agreement between JKR theory and both loading and unloading experiments [6,13]. In summary, considerable variations have been reported of which the origin could be either in the material or in the method. An important issue is to reach an equilibrium state both for the material and for the measuring apparatus. Several authors emphasize the need for 'quasi-static' experimental conditions, i.e. allowing the system sufficient time to reach equilibrium [9–13]. The requirements might be different for loading and unloading curves [16]. This 'asymmetry' arises because for loading the attractive surface forces at the crack tip are synergetic with the external load, which is not true anymore for unloading [12].

A lesser-investigated aspect is the possible correlation of adhesion and friction behaviours in PDMS. Though Galliano *et al.* considered this issue at a macroscopic scale [17], understanding friction behaviour at a mesoscopic level is still a major challenge. Regarding PDMS, measurements have been reported on the sliding friction of the PDMS on tethered brushes on a substrate [18,19] but not between two elastomer systems.

In the context sketched above, we developed a second-generation JKR instrument in order to take a fresh perspective on issues of adhesion and friction. The novelty of the instrument lies in its ability to perform fast experiments with great accuracy in a dynamic way. Additional features are the reliable determination of the associated indentation and the capability to investigate *in situ* the friction behaviour of the same sample. In the present paper we report a systematic study on the adhesion behaviour of PDMS as a function of molecular crosslink density and the presence of dangling chains. We reproduce the known decrease of the elastic modulus of PDMS with increasing molecular mass, and report a strong decrease upon addition of dangling chains. In contrast the work of adhesion turns out to be insensitive to these variations in the PDMS properties, indicating that the broken bonds are mainly internal to the system. Furthermore, we consider briefly various problems of hysteresis in relation to adhesion/adherence as well as of incorporating indentation data in the analysis. Finally friction results of the same samples are discussed, which indicate an increased friction force for a larger molecular mass, in contrast to published results for PDMS on self-assembled monolayers.

2. Summary of basic JKR theory

A typical JKR experiment consists of bringing into contact two samples in the shape of a lens (semi-sphere) and a sheet under the influence of an external load P that increases until P_{max} is reached and subsequently retracting them till the contact is broken (see Fig. 1). The deformation at a specific load P is described by the contact area (a circle of radius a), and the indentation in the sample δ as a result of the compression.
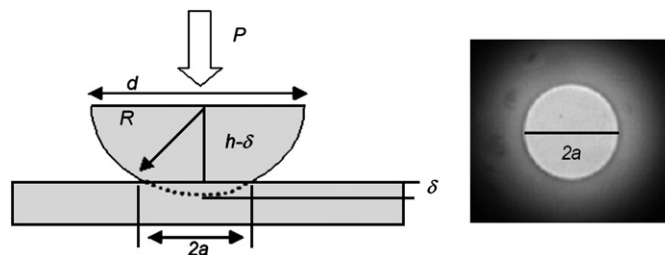

Fig. 1. Schematic representation of an elastic semi-sphere and a flat sheet in contact under a load P (left), along with an image of the contact area (right).

In the JKR model the elastic modulus K and energy release rate G of the system are derived from a and δ [2,3,6]. For a semi-sphere of radius of curvature R, the various parameters are related via

$$a^3 = \frac{R}{K}\left(P + 3\pi GR + \sqrt{6\pi GRP + (3\pi GR)^2}\right), \tag{1}$$

$$\delta - \delta_0 = \frac{a^2}{3R} + \frac{2P}{3aK}. \tag{2}$$

In this expression δ_0 is the zero point of the indentation measurement and K is the effective modulus given by

$$\frac{1}{K} = \frac{3}{4}\left[\frac{1-\nu_1^2}{E_1} + \frac{1-\nu_2^2}{E_2}\right] = \frac{9}{8E}, \tag{3}$$

where E_i and ν_i are the Young's modulus and the Poisson ratio of samples 1 and 2, respectively. The second equal sign applies to identical materials ($E_1 = E_2 = E$) for which in addition volume conservation is assumed ($\nu_1 = \nu_2 = 0.5$).

According to Eq. (1) the contact area reduces to zero only when P becomes negative. In that case a real solution to Eq. (1) exists for $6\pi GRP \leq (3\pi GR)^2$, in which the equality sign represents the limiting case of two bodies just in contact. Using this equality, the force necessary to separate the two bodies completely (the pull-off force, to be designated by the subscript PO) is given by

$$P_{PO} = \frac{3}{2}\pi GR. \tag{4}$$

For reversible contacts and quasi-static loading/unloading, G approaches the thermodynamic work of adhesion W. In mechanical equilibrium a value of G can be assigned to each point along the loading and unloading curves. For an advancing contact (loading) $W = G + \text{dissipation}$: W sets an upper bound to the acquired value of G. In contrast for a receding contact (unloading) $G = W + \text{dissipation}$ and W sets a lower bound to G. Hence G for unloading often exceeds the loading value and hysteresis is observed. For sufficiently slow rates of advance a limit of G close to W can be obtained [10]. For elastomers under unloading G is in principle a function of the crack velocity [16].

When for large deformations the bulk distortions reach the non-touching edges of the sample, effects of the finite size of either or both the lens and the sheet may become important.

This is particularly significant if the sheet consists of a glass or silicon plate with a thin grafted layer. Such finite-size corrections are second-order in Eq. (1) and first-order in Eq. (2). For a soft lens of thickness h (see Fig. 1) against a hard body (or the reverse) the latter equation then reads [2,20]:

$$\delta - \delta_0 \approx \frac{a^2}{3R} + \frac{2P}{3aK}\left(1 - \frac{a}{h}\right). \tag{5}$$

Obviously this correction is valid for $(a/h) \ll 1$ and vanishes for small loads (small a).
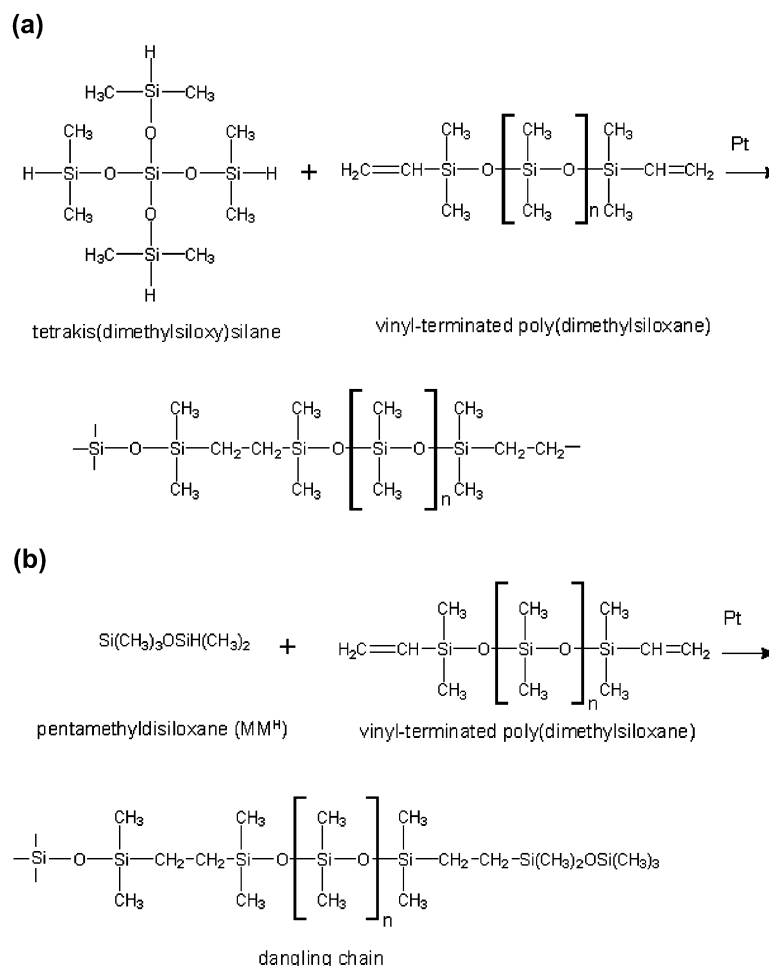
3. Experimental

3.1. Instrument

The JKR apparatus consists of two double leaf springs, one each for the vertical and horizontal forces, coupled to a single leaf spring unit. The vertical leaf spring is primarily used for adhesion investigations. The presence of the horizontal leaf spring allows studying friction behaviour on the same sample. The leaf spring unit is attached to an elastic hinge system that is capable of moving in the vertical and horizontal directions, using an ultra-high-resolution linear actuator (M-230 closed loop DC motor, Physik Instrumente). The hinge system can be moved with

a maximum speed of 1.5 mm/s at a minimum incremental motion of 50 nm. The vertical and horizontal leaf springs have a stiffness of $k_n = 1320$ N/m and $k_l = 360$ N/m, respectively. The system was calibrated by placing some small known masses on the leaf springs and recording the resulting displacements.

The JKR unit was mounted on an inverted transmission optical microscope. A digital camera with a CCD detector was used to record images of the contact interface. Typically a PDMS lens was attached to the sample holder on the vertical leaf spring with a sheet at the opposite surface. The motor and consequently also the leaf spring with the sample holder were moved down until contact of the samples. The resulting force and indentation were recorded using capacitive sensors positioned above and adjacent to the vertical and horizontal leaf springs, respectively. The set-up was placed on a vibration–isolation table in an air-conditioned room with controlled temperature and low humidity. Under these minimized ambient noise levels, the minimum force and displacement measurable were 15 μN and 15 nm, respectively.

3.2. Materials

PDMS elastomer samples were prepared by the standard hydrosilylation cross-linking reaction shown in Scheme 1

Scheme 1. Representation of (a) the hydrosilylation reaction and (b) the addition of a dangling chain.

[21]. The viscoelastic properties of such a polymer network are determined by its topology, which in turn is influenced by the number of crosslinks and M_c, the molar mass between crosslinks (see Fig. 2a). The latter quantity was varied between 6 and 28 kg/mol. The increase in length of the polymer chain with M_c is expected to decrease the density of crosslinks and consequently the elastic modulus of the sample [22]. An incomplete cross-linking reaction might result in imperfect networks, containing elastically ineffective chains that are free at one end. From infrared (IR) measurements, the conversion of the $-CH=CH_2-$ groups was found to vary between 95% and 98%. In addition dangling chains were introduced explicitly by adding pentamethyldisiloxane (MM^H) to the formulation. The unique SiH end of this molecule binds to a single vinyl end group of a PDMS chain, giving a dangling chain (provided the other chain end of PDMS is linked to the network) as shown in Fig. 2b. *A priori* such dangling chains were anticipated to act like connectors between the contacting surfaces. Different amounts of dangling chains can be quantified by the molar ratio MM^H/SiH as verified by IR. Table 1 gives the sample codes and the specification of the PDMS compositions studied. A more complete discussion of the chemical aspects will be given elsewhere [23].

Lenses were prepared by depositing droplets of a PDMS solution onto a fluorinated glass slide in a low-dust surrounding. Sheets with a thickness of about 1 mm were prepared by pouring the mixture into a flat-bottomed polystyrene petri dish. All samples were cured at 60 °C for 3 days under vacuum. Low-energy ion scattering indicated that the surfaces were free of contamination. Furthermore, the quality and smoothness of the samples were checked by optical and scanning force microscopies; the average surface roughness was ≤1 nm. The lenses were typically 0.6–1.0 mm in height with a radius of curvature in the range 1.5–2.2 mm. The height h and base width d were measured by imaging the side profile of the lens microscopically. Subsequently, the radius of curvature R of the lens was determined using the expression $R = h/2 + d^2/8h$. The overall measurements of R were reproducible within 3%.

3.3. Measurements

Following the classical JKR procedure, the contact radius a and the indentation δ were simultaneously measured as a function of the applied load P. The value of a was extracted
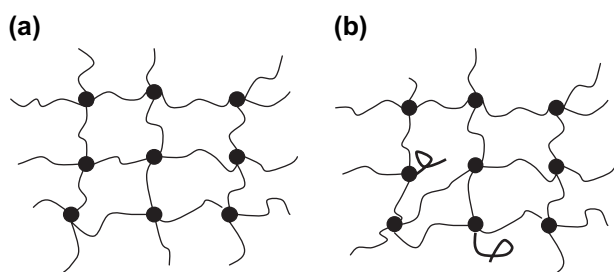

(a)　　　　　**(b)**

Fig. 2. Sketches of (a) a perfect model PDMS network and (b) the same in the presence of dangling chains.

Table 1
Characteristics of the samples investigated

Sample code	Molecular mass M_c (kg/mol)	Fraction of dangling chains (MM^H/SiH)
A_6	6	0
B_6	6	0.25
C_6	6	0.33
$A_{9.4}$	9.4	0
$B_{9.4}$	9.4	0.25
$C_{9.4}$	9.4	0.33
A_{17}	17	0
B_{17}	17	0.25
C_{17}	17	0.33
A_{28}	28	0
B_{28}	28	0.25
C_{28}	28	0.33

from the circular images (see Fig. 1) using software based on Hough Transformations developed by the Dutch Center for Image Processing, TNO Delft, The Netherlands. Elliptic corrections to the circles were investigated and found to be negligible. The maximum load applied was about 2 mN, which approached at an optimized motor speed of 0.2 μm/s corresponding to about 20 μN/s (to be discussed in more detail in Section 4.1). Under these conditions a had typically values up to 250 μm, leading to (a/h)-values up to about 0.25 (compare Eq. (5)). Finally, using the horizontal leaf spring the lateral frictional force was measured at a fixed normal force of ∼5 mN for various sliding velocities between 1 and 100 μm/s.

4. Results and discussion

4.1. Equilibrium and dynamic measurements

To address the issue of thermodynamic equilibrium during the measurements [9–13] we considered the high-M_c material A_{28} (see Table 1). This sample was assumed a priori to be most rate-sensitive because of the anticipated low modulus. The contact area was monitored over an appreciable period of time during which the load was increased in steps of about 0.2 mN with a waiting period of 40 min at each point. The observed variation in contact radius over this period was less than 3%. The variation in G as obtained from fitting each of the corresponding curves to Eq. (1) was less than 10%. Similar results were obtained for sample A_6.

In principle, keeping a waiting time at each step (quasistatic mode) is equivalent to changing the speed of loading. Using the samples A_{28}, B_{28} and C_{28} the loading speed was varied in the range 0.05–1 μm/s; unloading was done at a constant speed of 0.2 μm/s while there was no waiting at any point. Fig. 3a–c shows the resulting loading–unloading behaviours for these cases. The curves for different speeds superimpose very well; the results from fitting the loading curves are given in Table 2. Though the samples B_{28} and C_{28} show a slight tendency to lower values of W with increasing speed, these variations are well within the experimental accuracy of about
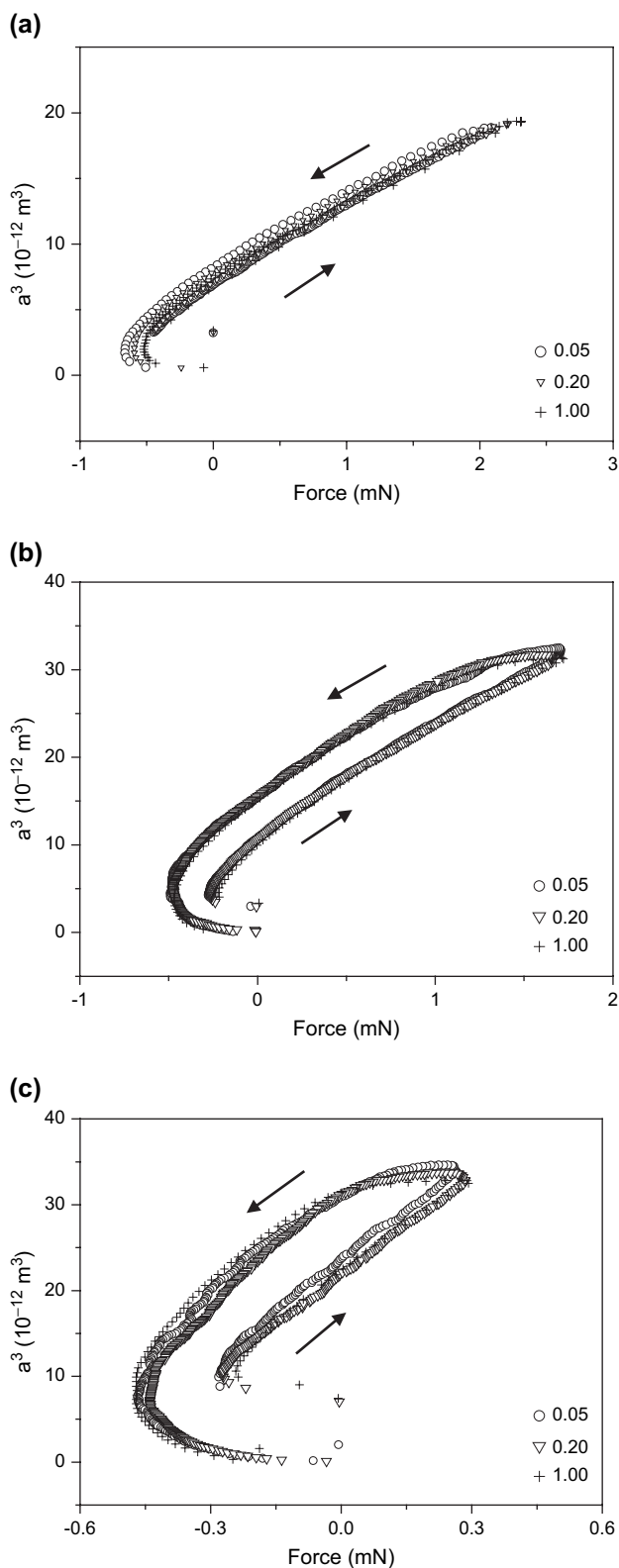
(a)

(b)

(c)

Fig. 3. Loading–unloading curves at different loading speeds as indicated in μm/s. (a) Sample A_{28}, (b) sample B_{28}, (c) sample C_{28}. Note that the force scales are different in order to maintain a comparable contact area.

$\pm 5\%$. Hence we assume that equilibrium has been reached and that the value obtained in this way for G can be taken as a rather accurate approximation for W. Evidently the contact area

Table 2
Values of E and W from fitting the experimental curves of Fig. 3a–c to Eq. (1)

Sample code	Speed (μm/s)	E (MPa)	W (mJ/m^2)
A_{28}	0.05	0.78	44
	0.2	0.80	46
	1	0.78	43
B_{28}	0.05	0.20	44
	0.2	0.22	43
	1	0.20	40
C_{28}	0.05	0.10	40
	0.2	0.11	39
	1	0.10	36

is established almost instantaneously. As in PDMS the responsible interactions are Van der Waals forces, one should be cautious in generalizing these results to other systems. For the subsequent experiments we adopted a protocol of loading–unloading the samples at a motor speed of 0.2 μm/s (about 20 μN/s).

4.2. Variation of elasticity

Measurements were performed on the full set of samples and both the loading (subscript L) and unloading (subscript UL) curves were fitted to Eq. (1). The resulting values of E and W are shown in Table 3. The observed decrease of E with increasing M_c conforms well to results reported in the literature [11,18,24,25]. It can qualitatively be understood in terms of a higher crosslink density in low-molecular-mass materials because of the shorter chain lengths. A simple estimate of the effect can be made using the classic equation of rubber elasticity [24]:

$$E = \frac{3\rho RT}{M_c}, \qquad (6)$$

where ρ is polymer density ($\sim 0.96 \times 10^3$ kg/m^3) and R and T are the gas constant and absolute temperature, respectively. The model is rather simple and should work only for perfect networks. A fit of the experimental data of series A to Eq. (6) is shown as curve a in Fig. 4. Though our networks could be

Table 3
Results of the JKR analysis for all samples listed in Table 1

Sample	E_L (MPa)	E_{UL} (MPa)	W_L (mJ/m^2)	W_{UL} (mJ/m^2)	W_{PO} (mJ/m^2)
A_6	1.16 ± 0.14	1.20 ± 0.17	45 ± 3	52 ± 3	50 ± 3
B_6	0.82 ± 0.14	0.84 ± 0.13	43 ± 2	52 ± 2	48 ± 2
C_6	0.56 ± 0.11	0.58 ± 0.11	43 ± 2	54 ± 3	52 ± 2
$A_{9.4}$	1.03 ± 0.05	1.04 ± 0.05	45 ± 3	51 ± 4	49 ± 3
$B_{9.4}$	0.54 ± 0.07	0.53 ± 0.07	40 ± 2	46 ± 3	47 ± 2
$C_{9.4}$	0.20 ± 0.01	0.20 ± 0.02	41 ± 2	54 ± 2	54 ± 2
A_{17}	0.93 ± 0.03	0.94 ± 0.04	44 ± 2	51 ± 3	50 ± 2
B_{17}	0.24 ± 0.05	0.25 ± 0.05	40 ± 1	63 ± 9	62 ± 7
C_{17}	0.16 ± 0.01	0.17 ± 0.01	42 ± 2	71 ± 8	71 ± 9
A_{28}	0.71 ± 0.14	0.71 ± 0.14	42 ± 3	52 ± 8	54 ± 6
B_{28}	0.21 ± 0.03	0.22 ± 0.03	44 ± 1	79 ± 7	71 ± 6
C_{28}	0.09 ± 0.03	0.09 ± 0.03	40 ± 2	58 ± 1	57 ± 1

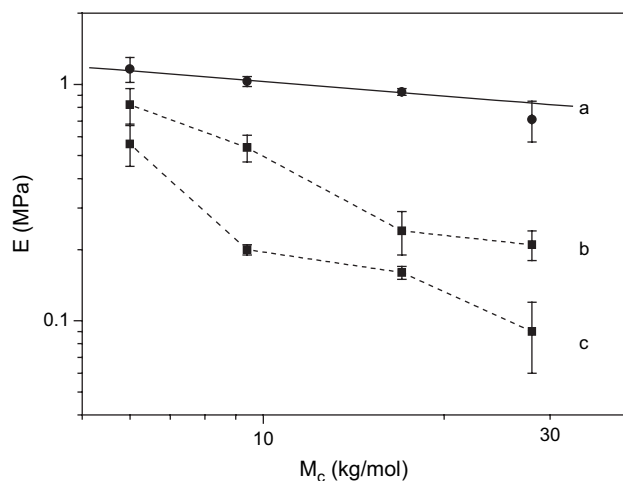The errors refer to the scatter in values over typically 10–15 samples.

Fig. 4. Dependence of the elastic modulus on the molecular mass: (a) sample series A with fit to Eq. (6); (b) series B; (c) series C. The dotted lines are for easy viewing only.

Fig. 5. Stability of G in the loading regime and hysteresis in the unloading regime in a typical experiment of self-adhesion of PDMS (sample A_{28}).

far from perfect, within the error bars the fit is reasonable and the results can broadly be construed to follow this simple model.

The elastic modulus also decreases upon addition of dangling chains, whose effect is much stronger than the influence of M_c. Dangling chains attached to the end of a PDMS sequence are expected to prevent complete crosslinking, resulting in strongly imperfect networks. The sketches in Fig. 2 give a simplified picture of how these networks might look, assuming complete reactions. Thus, the addition of dangling chains can be considered as equivalent to breaking of bonds in the load-carrying network, leading to a decrease of the elastic modulus. Amouroux and Léger [9] reported a similar trend for a much smaller variation in the concentration of dangling chains.

4.3. Adhesion and adherence

From Table 3 we note that all material variations hardly influence the work of adhesion. Fits of the loading curves lead to $W = 42 \pm 3$ mJ/m^2 in close agreement with values expected for PDMS [6,18] and equal to about twice the surface tension ($\gamma = 21.6$ mJ/m^2). We conclude that during loading the energy release rate is about equal to the work of adhesion, i.e. $G \approx W$. Fig. 5 shows typical variations of G calculated at each point during a full cycle, indicating a remarkable stability of G during the loading part. This result provides additional proof that indeed thermodynamic equilibrium has been reached in the dynamic mode used. Though the constancy of W with variation of M_c is known [18,26], the lack of influence of dangling chains is somewhat surprising. Chen et al. [26] indicate that the population of chain ends at the surfaces is the most important factor determining adhesion, and according to common views loose chain ends should preferably accumulate at the surface. Hence we conclude that in our PDMS systems the dangling chains are mainly made up of internally broken bonds. This is in agreement with the explanation given above of a decreased elastic modulus due to this effect.
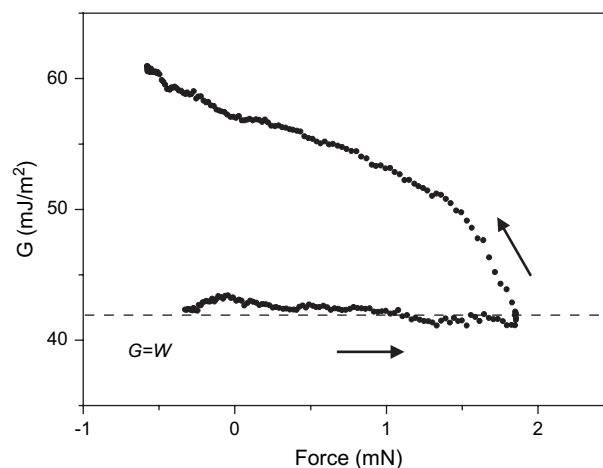
In addition to the determination of W from fitting the loading and unloading curves, the pull-off force has been determined. The resulting values (subscript PO) are given in Table 3 and indicate that $W_{UL} \approx W_{PO} > W_L$, implying hysteretic behaviour. These findings are qualitatively corroborated by Fig. 6a showing typical loading–unloading curves of samples with different molecular mass for which the hysteresis increases with M_c. The trend in hysteresis upon addition of dangling bonds is shown in Fig. 6b. The effect of dangling chains on the adherence of the material becomes more prominent with increasing M_c and is stronger than that of the molecular mass itself (see Table 3). These results suggest that increasing M_c has two effects: a lower cross-linking density (larger chain length between chemical nodes) and an increased number of pendant chains (linked to the network by only one extremity). The second effect is reinforced by the addition of dangling chains. The combined effects result in a lower elastic modulus and higher adherence.

Apart from the material properties also the experimental conditions contribute to the adherence [11,24]. A more quantitative treatment would require further systematic work controlling precisely the velocity of the contact line. Such studies have been reported for a single mass of about 16 kg/mol [9] and confirm the trend presented here. In addition a dependence of the adherence on the waiting time between loading and unloading was observed.

4.4. Fitting indentation data

Eq. (2) relating the indentation, force and contact area is independent of W and can be used to check the self-consistency of JKR model. Limiting us in this section to samples with different molecular mass, a typical case comparing the measured indentation with the one calculated from Eq. (2) is shown in Fig. 7. To obtain the calculated curve the value of E from the JKR fit [Eq. (1)] was used as input in Eq. (2) to predict the indentation data. The agreement between the measured and calculated curves is very reasonable. In Table 4 E-values are
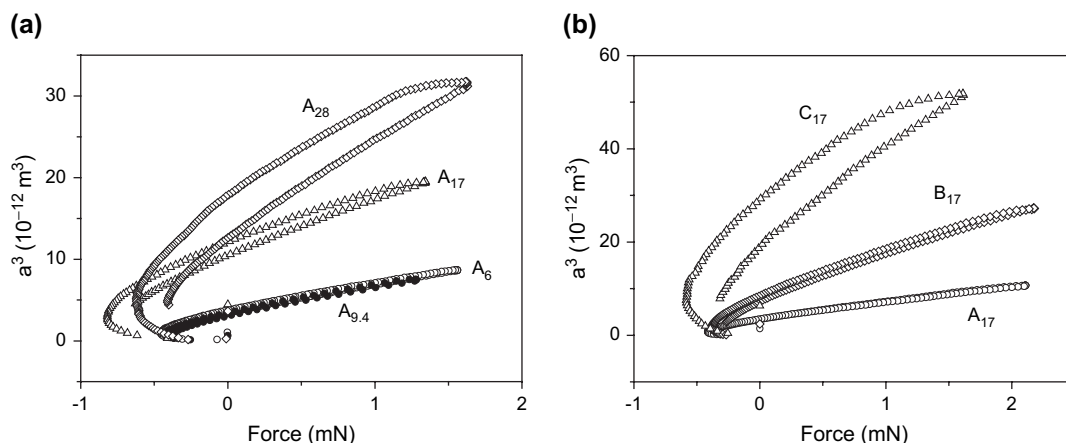
(a)

(b)

Fig. 6. Influence of (a) molecular mass between crosslinks and (b) addition of dangling chains on the hysteresis behaviour of PDMS. The number of data points has been reduced for clarity.

compared from fitting the loading curve using Eq. (2) (designated as E_δ) and from the direct JKR fit to Eq. (1). The latter data E_L are from Table 2. We note that the two methods are reasonably consistent for these averages over a relatively large number of experiments. However, even though in the majority of cases the differences are within 10−20% and sometimes perfect agreement is reached as in Fig. 7, in several individual cases the discrepancy can be as large as 30−40%. Though this effect is rather common in the literature [5] the reasons for this unpredictability of the indentation data are not clear. Our results on any particular sample are reproducible when the experiment is repeated after remounting, thereby ruling out improper mounting of samples resulting in uneven stress fields.

We considered the possibility of introducing corrections for the finite size of the samples as proposed by some authors [9,20]. However, according to Eq. (5) finite-size corrections should depend on the applied load via the factor a/h, in which h is constant and a is proportional to the load. As demonstrated in Fig. 5, the results for G for various loads do not show any indication of such a variation. Furthermore, any type of
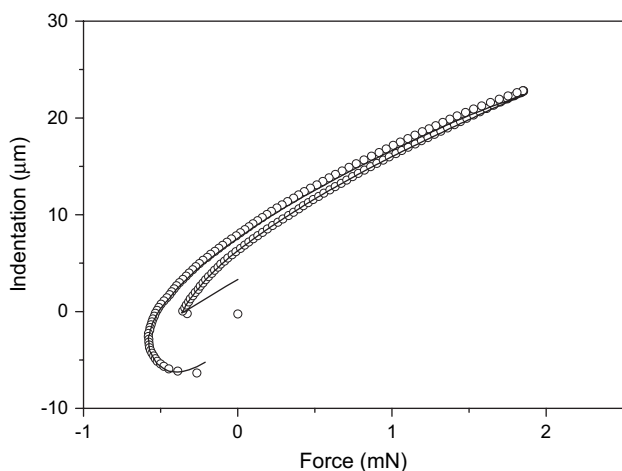

Fig. 7. Typical indentation data of an A_{28} sample for which excellent agreement between the measured values (circles) and calculated ones (solid line) has been reached.

correction that would reduce the difference observed between the two approaches in a particular case should also be applied to other similar samples. This would spoil the agreement that has also often been observed. Hence our experiments provide no evidence that in the present situation of self-adhesion finite-size corrections are of any importance. According to Amouroux and Léger [9] such corrections are essential if adhesion is investigated against a thin film on a substrate.

We conclude that indentation data can provide valuable supplementary information to the classical JKR analysis and potentially allow determining E and W independently. However, so far no full consistency has been reached. We speculate that the indentation data are more sensitive to the detailed geometry of the samples, which might deviate from the ideal perfect semi-sphere and/or absolute flat sheet. This possibility requires a further in-depth analysis that is outside the scope of the present investigations.

4.5. Friction

In this final section we present experiments of the sliding friction of PDMS with two different M_c-values (samples A_6 and A_{28}) against the same material. So far measurements of the sliding friction of PDMS have focused on PDMS lenses against either glass [17] or tethered brushes on a substrate [18,19]. The lateral frictional force is shown in Fig. 8 for various sliding speeds, the corresponding adhesion behaviour has already been given in Fig. 6a. To the best of our knowledge these results constitute the first measurements of friction on samples in the same geometry as used to determine adhesion. The normal force of about 5 mN leads for sample A_6

Table 4
Comparison of values of E obtained by fitting to Eqs. (1) and (2)

Sample	E_δ (Eq. (2))	E_L (Eq. (1))
A_6	0.94 ± 0.10	1.16 ± 0.14
$A_{9.4}$	0.91 ± 0.05	1.03 ± 0.05
A_{17}	0.84 ± 0.02	0.93 ± 0.03
A_{28}	0.60 ± 0.11	0.71 ± 0.14

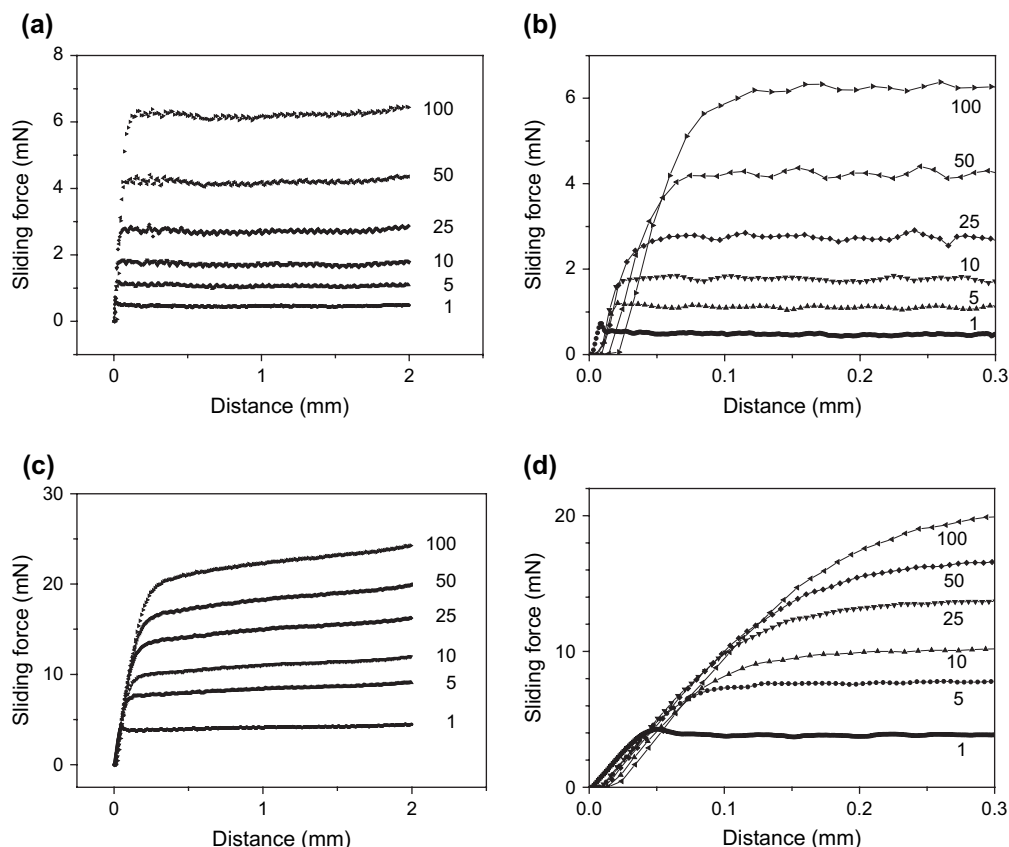The errors refer to the scatter in values over typically 10−15 samples.

Fig. 8. Lateral sliding force of sample A_6 (a, b) and sample A_{28} (c, d) under a normal load of 5 mN at various sliding speeds (in μm/s) as indicated. Graphs (b) and (d) highlight the initial slope of graphs (a) and (c), respectively. Both slopes have a value of about 0.11 N/mm.

($E \approx 1.2$ MPa) to a contact area of about 0.25 mm^2 and for sample A_{28} ($E \approx 0.7$ MPa) to 0.37 mm^2. The contact area remains approximately constant during the sliding process. As a result the normal stress is 20 kPa and 14 kPa for samples A_6 and A_{28}, respectively. The friction data show a clear distinction between the initial stages of the sliding for which the friction force increases strongly with sliding distance ('static' friction) and the saturated part reflecting a dynamic regime.

Let us first consider the initial stages (Fig. 8b and d) for which the slope of sliding force against distance hardly depends on the velocity and has the same value of about 0.11 N/mm for both samples. As the respective contact areas differ, evidently also the shear stresses are at variance. Hence any diversity of the two samples under the same load is effectively translated into a variation of the contact area via the difference in elasticity. As a result no connection can be made between static friction and adhesion/adherence. In fact from Table 3 there is little reason to expect that, as both the adhesion and adherence are very similar for both samples. In contrast the friction force at the plateau region is strongly dependent on the speed as illustrated in Fig. 9. In addition the plateau value for the large-M_c sample A_{28} is a factor of 3 larger than that of the low-M_c sample A_6. In this context we note that Gordon *et al.* reported that the viscoelastic losses of several crosslinked PDMS networks also increase with molecular mass [27]. As far as friction is caused by bulk

dissipation this points to a lateral force that increases with M_c, which is exactly what we observe. This suggests a possible relation with the larger hysteresis in the JKR curve for A_{28} compared to A_6 (see Fig. 6a).

Our result of the sliding force being larger for A_{28} compared to A_6 contrasts strongly with the observation by Vorvolakos and Chaudhury [18] that the friction *decreases* with molecular mass. Several reasons could possibly account for this difference. First their data refer to PDMS against
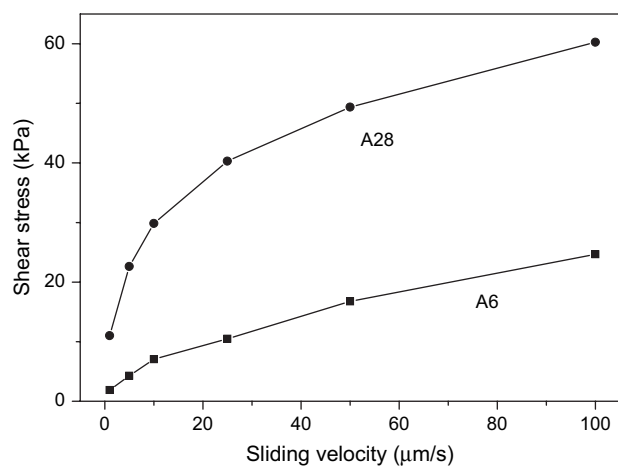

Fig. 9. Shear stress of samples A_6 and A_{28} as a function of sliding velocity at a fixed distance of 1 mm.

a self-assembled monolayer while we consider friction against the same material. Second we note that their relation has been tested up to $M_c \approx 16$ kg/mol, while our sample A_{28} is well above this value. Finally their relation is mainly based on data at relatively large sliding velocities (0.1—100 mm/s) in contrast to the present ones (1—100 μm/s). Interestingly Galliano *et al.* indicate at the end of their paper a reversal of the relation between friction and M_c when measured at smaller scales [17].

5. Conclusions

We have reported on the adhesion and friction of PDMS as determined by a newly developed JKR apparatus. Measurements in the so-called 'dynamic' mode of the system appear to be in thermodynamic equilibrium even at relatively high access speeds. We reproduce the known decrease of the elastic modulus of PDMS with increasing molecular mass. In addition a strong decrease is found upon addition of dangling chains. These variations of PDMS leave the work of adhesion largely unaffected at $W = 42 \pm 3$ mJ/m^2. This can be understood if the broken bonds are mainly internal to the system.

Indentations have been measured, leading to independent values of the elastic moduli that can be compared with the results of the JKR analysis. The two methods are reasonably consistent when averaged over a number of experiments. For the situation of self-adhesion possible corrections for the finite sample size are not relevant.

The present instrument allows measuring *in situ* friction forces on the same samples. Initial results on PDMS against the same material indicate an increased friction force for a larger molecular mass, in contrast to published results for PDMS against self-assembled monolayers. We speculate that this is due to bulk viscoelastic dissipation in agreement with the larger hysteresis in the JKR curve.

Acknowledgements

References

[1] See, for example: Barquins M, Maugus D. J Adhes 1981;1353, and references therein.
[2] Johnson KL, Kendall K, Roberts AD. Proc R Soc London A 1971; 324:301.
[3] Chaudhury MK, Whitesides GM. Langmuir 1991;7:1013.
[4] Shull RK. Mater Sci Eng 2002;R36:1.
[5] Oláh A, Vansco GJ. Eur Polym J 2005;41:2803.
[6] Crosby AJ, Shull KR. J Polym Sci Part B Polym Phys 1999;37:3455.
[7] Choi GY, Kim S, Ulman A. Langmuir 1997;13:6333.
[8] Silberzan P, Perutz S, Kramer EJ. Langmuir 1994;10:2466.
[9] Amouroux N, Léger L. Langmuir 2003;19:1396.
[10] Deruelle M, Léger L, Tirrell M. Macromolecules 1995;28:7419.
[11] Choi GY, Zurawsk W, Ulman A. Langmuir 1999;15:8447.
[12] Kim S, Choi GY, Ulman A, Fleischer C. Langmuir 1997;13:6850.
[13] Kim S, Choi GY, Nezaj J, Ulman A, Fleischer C. Macromol Symp 1997; 126:1.
[14] Oláh A, Hillborg H, Vancso GJ. Appl Surf Sci 2005;239:410.
[15] Pickering JP, van de Meer DW, Vansco GJ. J Adhes Sci Technol 2001; 15:1429.
[16] Deruelle M, Hervet H, Jandeau G, Léger L. J Adhes Sci Technol 1998; 12:225.
[17] Galliano A, Bistac S, Schultz J. J Adhes 2003;79:973.
[18] Vorvolakos K, Chaudhury MJ. Langmuir 2003;19:6778.
[19] Bureau L, Léger L. Langmuir 2004;20:4523.
[20] Shull KR, Ahn D, Mowery CL. Langmuir 1997;13:1799.
[21] See, for example: Thomas DR. In: Clarson SJ, Semlyen JA, editors. Siloxane polymers. Englewood Cliffs: Prentice Hall; 1993 [chapter 12].
[22] See, for example: Clarson SJ, Mark JE. In: Clarson SJ, Semlyen JA, editors. Siloxane polymers. Englewood Cliffs: Prentice Hall; 1993 [chapter 13].
[23] Li, Z. et al., in preparation.
[24] Carré A, Shanahan MER. J Colloid Interface Sci 1997;191:141.
[25] Li Z, Brokken-Zijp JM, de With G. Polymer 2004;45:5403.
[26] Chen N, Maeda N, Tirrell M, Israelachvili J. Macromolecules 2005; 38:3491.
[27] Gordon GV, Owen MJ, Owens MS, Perz SV, Stasser J, Tonge JS. Annu Meet Adhes Soc 1999;424.